IOSR Journal of Applied Geology and Geophysics (IOSR-JAGG)
e-ISSN: 2321–0990, p-ISSN: 2321–0982. Volume 14, Issue 3 Ser. 1 (May – June 2026), PP 09-22
www.iosrjournals.org

Application Of Aeroradiometric Data To Delineate The Hydrothermal Alteration Zones For Gold Exploration And Surface Geology In Parts Of Northwest Nigeria Schist Belt

Abdullahi, H.A. And Akpaneno, A.F.
Department Of Geophysics, Federal University Dutsin-Ma, Nigeria.

Abstract
The study applies high-resolution aeroradiometric data to map hydrothermal alteration zones for gold exploration and delineated surface geology in parts of the northwest Nigeria schist belts. The work uses eight NGSA radiometric sheets covering parts of Zamfara State and adjoining parts of Sokoto and Kebbi. Processing and map production were completed in Oasis Montaj software, followed by GIS-based interpretation and integration. Individual radioelement maps for %K, eTh, and eU were generated, then three hydrothermal alteration indicators were computed: K/Th ratio, F parameter, and potassium deviation (Kd). A fuzzy logic weighted overlay combined the three indicators into a composite hydrothermal alteration potential map classified into low, moderate, and high zones. Results show broad low alteration across the west and northwest, with stronger alteration concentrated in the central to eastern belt around Bukwium, Tashar Taya, Gwashi, Anka, Kagara, Dogon Daji, Tuduki, Gidan Garba, Dan Gulbi, and Surimi. Many high zones form elongated trends consistent with structural control. Validation through overlay of eight active mining sites shows six sites, 75%, located within high alteration zones, while the remaining sites align with mapped structures. Ternary RGB and CMY radiometric composites supported lithologic discrimination and aided digitising an updated surface geologic map of the area.

Keywords: *aeroradiometric mapping, hydrothermal alteration, gold mineralisation, fuzzy logic weighted overlay and schist belts.*

Date of Submission: 05-05-2026 Date of Acceptance: 15-05-2026

I. Introduction

The hydrothermal alteration processes entail the infusion of hydrothermal fluids with chemical compositions that vary according to the ratio of rock to fluid (Chen *et al*., 2025; Ondrejka *et al*., 2025; Tulepbayev *and* Tulemissova, 2025; Zaccarini *et al*., 2025; Green, 2023). This is later succeeded by the diagenetic alteration and remobilisation of mineral deposits through assimilation in host rocks under optimal temperature and pressure conditions. This subsequently induces alterations in the magnetic fabric, chemical composition, and mineralogy of rocks (Tulepbayev and Tulemissova). This enables the identification of abnormal alterations in rocks resulting from hydrothermal processes through geophysical techniques (Sanusi and Amigun, 2020). The delineation of hydrothermal alteration zones can be achieved by radiometric and magnetic techniques (Airo, 2002; Sabins, 1999; Nabighian *et al*., 2005). The radiometric method provides the most comprehensive information regarding the discovery and identification of alteration minerals that serve as markers for delineating hydrothermal alteration zones (El Cheikh *et al*. 2025; Ohwo and Solape 2024; Akinlalu, 2023; El-Qassas *et al*., 2023; El-Desoky *et al*., 2022). The identification of areas with elevated potassium levels can serve as a key indicator of gold mineralisation. This can be effectively determined through the presence of radioelements like Potassium (K), Thorium (Th), and Uranium (U) (Bello *et al*., 2025).

The radiometric method proves more effective in defining surface geology (Aliyu *et al*. 2025; Bello *et al* 2025; Doorn and Carter, 2025; Murphy, 2025). Numerous studies have shown that potassium concentrations in highly mineralised zones are typically about twice as high as those in non-mineralised areas. This potassium enrichment has been shown to be in a pattern that is linked with ore deposits. Throughout magmatic evolution, potassium becomes increasingly concentrated, leading to elevated potassium concentrations in felsic rocks relative to mafic igneous rocks. Basalt typically has K content variations of approximately 1%, while granite displays concentrations between 2% and under 6% (Akame *et al*., 2020; Yılmaz, 2019; Saikia *et al*., 2014; Ratajeski *et al*., 2001; Pe-Piper *et al*., 1994). The principal deposits containing potassium are diminished during the weathering process in the order of biotite, K-feldspar, and muscovite (Chen, 2009; Oyarzabal *et al*., 2009; Banfield, 1985; Stoch *and* Sikora, 1976). A decrease in Th and an increase in K indicate alterations in the

conditions of an ore deposit (Meng, 2013; Rao, 2012; Moxham *et al*., 1965; Pliler and Adams, 1962). Thorium is typically resistant to alteration processes, remaining stationary during mineralization or experiencing only partial depletion in areas of intense K-alteration and silicification (Nisbet *et al*., 2019; (Gao *et al*., 2017; Macdonald *et al*., 2017; Meng, 1999; Moxham *et al*., 1965). The K/Th ratio is therefore a more effective predictor of hydrothermal alteration than any one radioelement (Gobashy *et al*., 2024; Mamudu *et al*., 2024; Akinlalu, 2023; Azzazy, 2023; Egwuonwu *et al*., 2023).

Despite the high mineral potential of the Nigerian Schist Belt, systematic mapping of hydrothermal alteration zones is still limited. Most available geological maps are regional and too coarse for modern exploration targeting. Field mapping alone also fails to define subsurface alteration patterns in many places, since regolith cover and dense vegetation often hide bedrock exposures. Hydrothermal alteration zones, which often control gold mineralisation, can be identified by changes in natural radioelement concentrations, notably increased potassium and reduced thorium contents**.** However, these variations are not visible in the field without geophysical assistance. Therefore, there is a need for a quantitative, remote geophysical approach that integrates aeroradiometric data and GIS-based analysis to accurately delineate alteration zones. The lack of integrated geospatial products has reduced the effectiveness of gold exploration in the northwestern schist belt region.

Radiometric data has been employed in Nigeria, Africa at large and other parts of the world to map out lithology and delineate hydrothermal alteration zones (Tawey *et al*., 2021). Airo (2002) pointed out that alterations or changes in potassium (K), thorium (Th), and uranium (U) concentrations showcase the effects of hydrothermal alteration, weathering, and structural influences. Akinlalu (2023) and Mamudu *et al*. (2024) utilised aeroradiometric data in the Ife Ilesa Schist Belt and Bauchi region, respectively, discovering that elevated K/Th ratios and F parameter values are promising indicators. The works showed that using integrated radiometric datasets in a GIS environment improves the accuracy of alteration mapping compared to when only a single element layer is used.

The aim of this study is to delineate the hydrothermal alteration zones within parts of the northwest Nigeria schist belt using aeroradiometric data for gold exploration and surface geological mapping. These were achieved by producing a ternary radiometric map from gridded K, eU, and eTh data for the surface geology delineation. The geologic map of the portion (Figure 1) served as a reference for the identification of surface geologic boundaries. This was accomplished by providing support for the interpretation of radiometric fingerprints and radioelement ratio patterns, which were utilised to differentiate between the dominant rock groups (Mamudu *et al*., 2024; Tawey *et al*., 2021). We used high K/Th values to delineate zones of potassic alteration linked to hydrothermal mineralisation and exploration targets. We used the F parameter to highlight anomalous potassium enrichment relative to expected lithological background as evidence of hydrothermal alteration. Furthermore, the potassium deviation (Kd) map was generated to define areas of potassium enrichment or depletion relative to local background levels, as these Kd anomalies strengthen delineation of hydrothermal alteration footprints and we integrate K/Th ratio, F parameter, and Kd maps in a GIS using the fuzzy logic method to produce a composite hydrothermal alteration potential map of the area showing high, moderate, and low prospectivity zones for parts of the northwest Nigeria schist belt.

II. Location And Geology Of The Study Area

The area of interest is in northwest Nigeria, comprising sections of the Basement Complex and the Sokoto Basin (Figure 1). It is situated within portions of the Nigerian schist belts (NW) and bordered by latitudes 04º 30′ N and 06º 30′ N and longitudes 11º 00′ E and 12º 30′ E (Figure 1). This study area covers the northwest of Tambawa in the northwest, the northeast of Maru in the northeast, the southwest of Lumu in the southwest, and the southeast of Dan Gulbi in the southeast. The area covered mostly includes Zamfara State and somewhat extends into the southern areas.

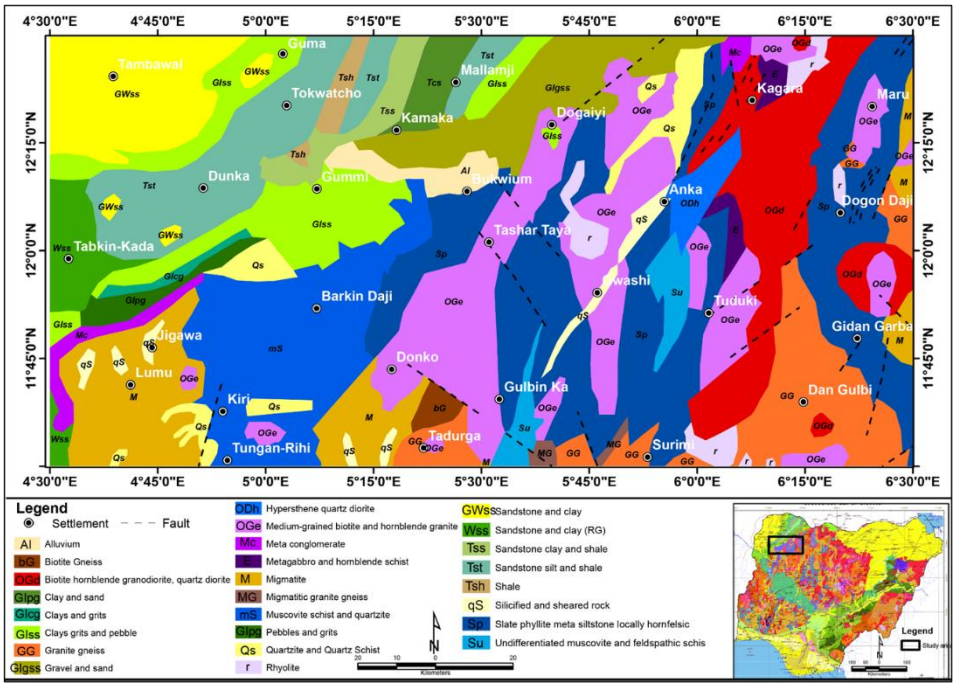

Figure 1: Location and geologic map of the study area (Modified from NGSA, 2006)

of Sokoto State and Kebbi State. The research location comprises the basement and sedimentary rocks and is tectonically positioned within the Pan-African mobile belt (Wright, 1985). The sedimentary segment delineates the southern edge of the Iullemeden basin, commonly known as the Sokoto basin. Abaa (1983) asserted that the deformational event referred to as the Pan African occurred in this region, resulting in regional metamorphism and the emergence of migmatite, granite, and gneiss. The basement rocks of Nigeria have four components (Obaje, 2009): the MGC, schist belts, older granites, and undeformed acid and basic dykes. The Schist Belts are a territory in Nigeria distinguished by low-temperature metamorphosed sediments, aligned in a north-south orientation in the northwest of the entire country. The rocks date to the Upper Proterozoic era and are linked to the MG complex. Some rocks may contain remnants of the ocean floor from small back-arc basins. Grant (1978) asserts the presence of numerous deposition basins, although McCurry (1976) views the schist belts as remnants of a unique supracrustal layer. Both individuals consider these rocks to have originated from faulted rift-like formations. Turner (1983) contends that sediment ages vary according to structural and lithological relationships. Ajibade *et al*. (1979) challenge this conclusion, demonstrating the series underwent equivalent deformation histories. Truswell and Cope (1963) considered the structural relationships between the schist belts and the basement to be conformable, but Ajibade *et al*. (1979) recognised it as a structural discontinuity. Figure 1 also depicts the geological formations present in the study area. The chronological dating of the different rocks within this habitat remains contentious; nonetheless, the older granites suggest a minimum age of approximately 750 Ma. The dates of the amphibolite complexes inside these rocks have also generated discussion. Ajibade *et al*. (1979) predominantly supported ensialic mechanisms in the formation of schist belts, although Egbuniwe (1982) observed that some contain oceanic components with tholeiitic characteristics. The rocks have been surveyed, and the information has been disseminated. Documented locations of schists in Nigeria include Maru, Anka, Zuru, Kazaure, and others, where the rocks are recognised to contain or host gold and other identified solid minerals. Within the study area, three prominent schist belts, Maru, Anka, and Zuru, are found, alongside about twenty-six (26) distinct rock types represented in the location (Figure 1).

III. Material And Methodology

The Nigerian Geological Survey Agency (NGSA) in Abuja provided eight radiometric data sets for the study area: 50 (Tambawal), 51 (Gummi), 52 (Anka), 53 (Maru), 73 (Fokku), 74 (Donko), 75 (Gwashi), and 76 (Dan-Gulbi). This study was carried out from 2005 to 2009, funded by the Nigerian Federal Government and the World Bank. The survey was conducted in two phases. The Nigerian government completely financed the initial phase, during which Fugro Aerial Surveys conducted all aerial geophysical data gathering, processing, and interpretation (Reford *et al*., 2010). Phase 1 included 826,000-line kilometres of magnetic and radiometric surveys and 24,000-line kilometres of time-domain electromagnetic surveys. Phase 2, finalised in August 2009, encompassed 1,104,000-line kilometres of surveys, facilitated by the World Bank, with data collecting and compilation overseen by Fugro Airborne Surveys.

The ternary map of the study area was produced within the Oasis Montaj version 8.3 environment, after which it was exported as a GeoTIFF file and imported into the GIS environment and was digitised to produce the surface geologic map of the area. Furthermore, the identification of potassium enrichment zones associated with hydrothermal alteration that may include orogenic gold mineralisation and other minerals in the research area was conducted utilising three (3) methods displayed in Table 1.

Also, the derived radiometric maps; K/Th ratio map, F-parameter map, and K deviation map (Table 1), were integrated within the Geographic Information System (GIS) environment. Applying the fuzzy logic weighted overlay (Akinlalu 2023). This integration produced a final composite hydrothermal alteration zone map that delineates areas with high, moderate, and low potential for gold mineralisation, providing a reliable framework for future exploration activities in the parts of the northwest Nigeria schist belt.

Table 1: Showing hydrothermal zone delineation equations and sources

S/N	Name	Formular	Source
1	Ratio of eTh to %K	$\left(\frac{K}{eTh}\right)$	Portnov (1987)
2	F-parameter	$F = \frac{K * eU}{eTh} = \frac{K}{\frac{eTh}{eU}} = \frac{eU}{\frac{eTh}{K}}$	Efimov, (197
3	K deviation	$K_d = \frac{K - K_n}{K_n}$ $K_n = \left(\frac{K\ map_{average}}{Th\ map_{average}}\right) * Th\ map$	Saunders *et al.* (1987)

IV. Results And Interpretation

Potassium (%K), thorium (eTh) and uranium (U) maps

Figure 2 represents the potassium percentage map, while Figure 3 represents the equivalent thorium map, and Figure 4 represents the equivalent uranium map. From Figure 2, the %K map shows potassium values of about 0.165 to 2.552%, with low K in the west and northwest around Tambawal, Tabkin Kasa, and Jigawa; moderate K across the central belt around Barken Daji, Donko, and north of Tadurga; and high K concentrated in the east and southeast around Anka, Tuduki, Kagara, Maru, and Dogon Daji.

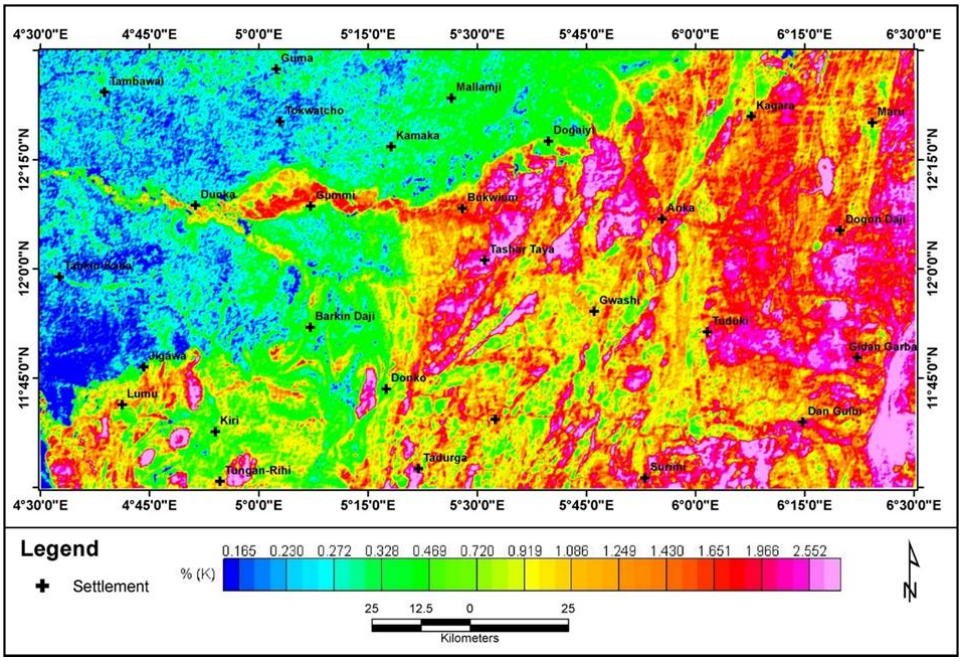

Figure 2: Percentage Potassium (%K) Map

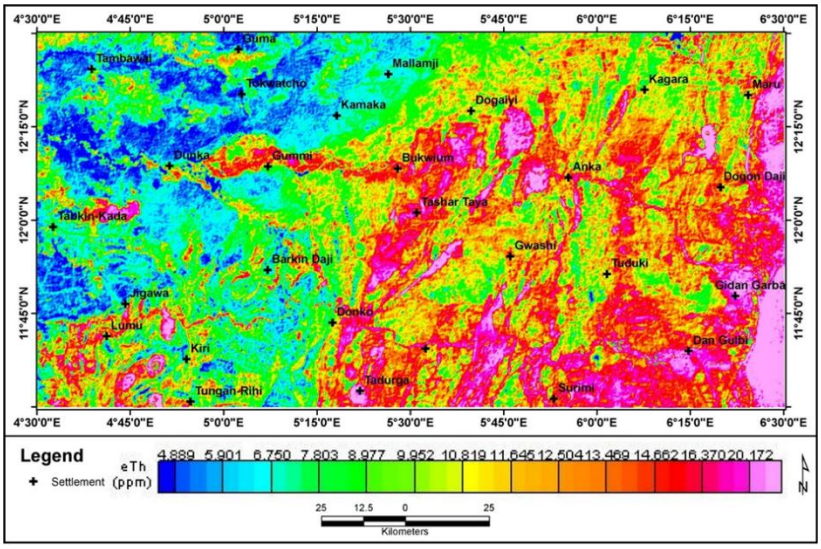

Figure 3: Equivalent Thorium map

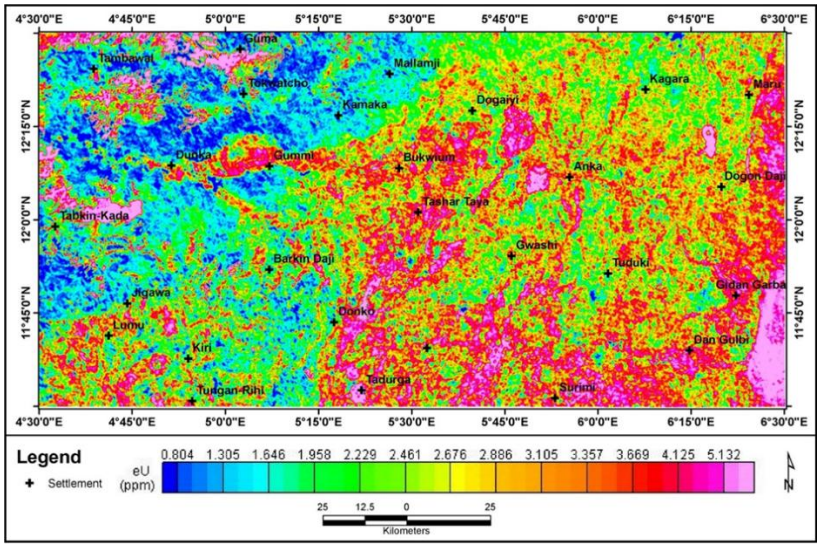

Figure 4: Equivalent Uranium (eTh) map

and Gidan Garba, including a linear high-K corridor from west of Dunka through north of Gummi toward Bukwium and several elongate high-K bands that suggest K-rich felsic rocks, pegmatite or potassic alteration controlled by the structure of the NE-SW trend (Figure 2). The eastern portion of the study area is specifically basement (Figure 1), and this confirms the concentration of potassium in this location so also is the west and the northwest that is predominantly sedimentary rocks that have low K concentration.

The eTh map (Figure 3) shows thorium values of about 4.889 to 20.172 ppm, with low eTh dominating the west and northwest around Tambawal, Tabkin Kasa, Tokwatcho, and Jigawa; moderate eTh forming a broad central belt around Barken Daji, Donko, Kamaka, and Mallamji; and high eTh concentrated in the east and southeast around Bukwium, Tashar Taya, Dogaiyi, Anka, Kagara, Maru, Dogon Daji, Tuduki, Dan Gubi, and Gidan Garba, where several elongated high eTh trends mostly in the NE-SW direction occur, implying thorium-rich felsic granitoids, pegmatites, or radiogenic metasediments (Figure 1) in the east versus more mafic or quartz-rich units in the west. For the alteration screening pattern, we can compare Figure 3 with Figure 2; this is because on the %K map, zones with high K but relatively lower eTh stand out as potassium enrichment against the local background.

The uranium (eU) map (Figure 4) presents the distribution of equivalent uranium concentration across the area, from about 0.804 to 5.132 ppm, where dark blue to light blue colours represent low eU and yellow to pink colours represent high eU. Low eU dominates the western and northwestern blocks around Tabkin Kada, Jigawa, Tambawal, Suna, and Tokwatcho, while moderate to high eU spreads across the centre and east, with prominent highs forming pink patches and elongated belts around Gummi, Bukwium, Tashar Taya, Dogaiyi, Anka, Gwashi, Tuduki, Surimi, Dan Gulbi, Gidan Garba, Dogon Daji, and the Maru flank. This eastward increase

and the clustered highs suggest uranium enrichment linked to felsic basement lithologies, pegmatite and granitic bodies in this location (Figures 1 and 4), or alteration zones where fluids concentrate radioelements along fracture corridors. The mottled green to yellow background marks mixed lithologies or variable regolith thickness, while the blue domains mark low uranium content (Sediments), possible thicker cover, or less radioactive rock types.

Hydrothermal Alteration Zones

Several studies have shown that potassium enrichment or hydrothermal alterations are markers of hydrothermal orogenic gold mineralisation processes (Bello *et al.,* 2025; El Cheikh *et al.,* 2025; Akinlalu, 2023; El-Desoky *et al.*, 2022; Tawey *et al.,* 2021; Sanusi and Amigun, 2020; Cunha *et al*., 2017; Airo, 2002*).* As a result, portions of potassium enrichment highlighted by the radiometric data have been utilised to delineate hydrothermally altered areas within the study area employing the K/Th, K deviation map, and the F-parameter maps (Figures 5, 6 and 7). These delineated hydrothermal areas, represented by several black polygonal lines that captured areas that have been affected by hydrothermal activities and may host orogenic gold mineralisation, have been merged to produce the composite hydrothermal alteration map of the study area (Figure 8).

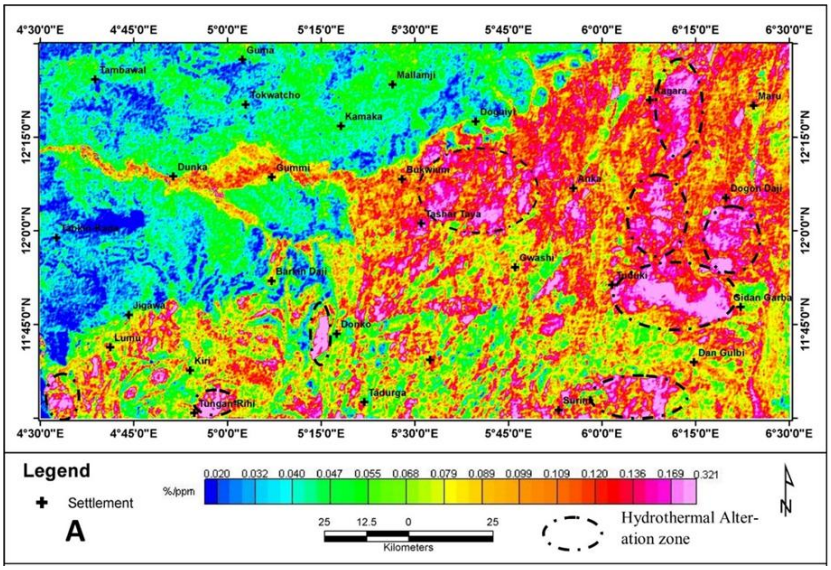

Figure 5: K/Th ratio map

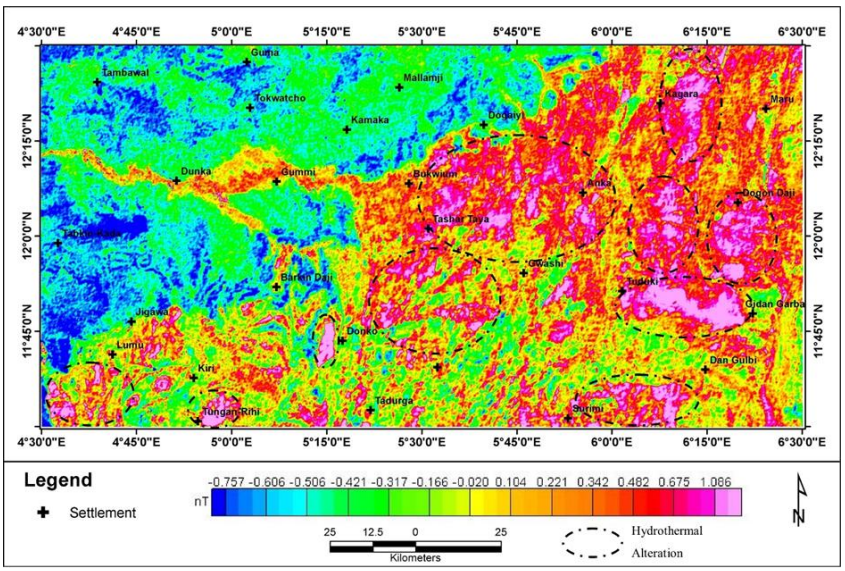

Figure 6: Potassium (K) deviation (K_d) map

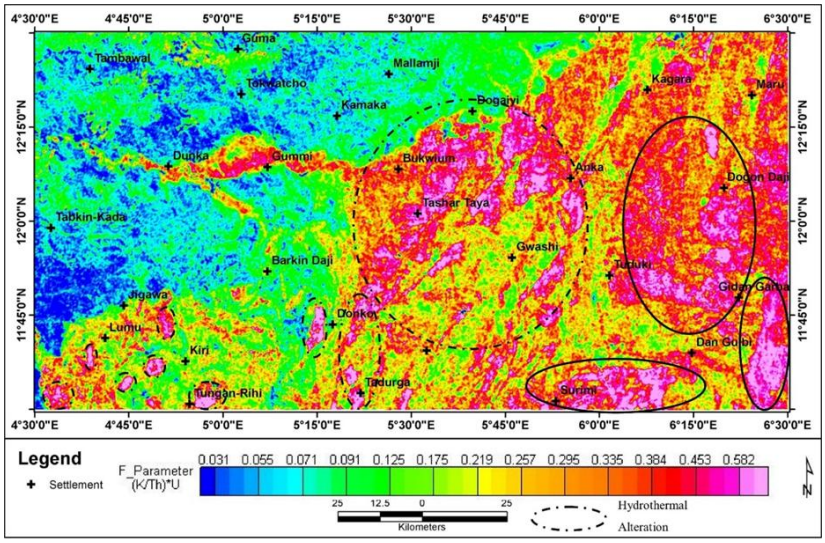

Figure 7: F-Parameter Map

Potassium-Thorium (K/Th) Ratio Map

Figure 5 represents the K/Th map of the study area, where deep to light blue portions represent low hydrothermal zones, yellow zones represent moderate alteration values, and red to pink zones represent high alteration values. Since thorium tends to remain stable during alteration while potassium increases when hydrothermal fluids introduce potassium-rich minerals such as K-feldspar and sericite, elevated K/Th values serve as a strong indicator of potassic alteration (Qiu *et al*., 2024; Akinlalu 2023; Boadi *et al.*, 2022; El-Sadek, 2022; Santiago Ramos *et al*., 2022; Zhang *et al*., 2022; Elkhateeb *and* Abdellatif, 2018; Macdonald *et al*., 2017; Chiozzi *et al.,* 2008; Airo, 2002; Shives *et al.,* 1995; Cathelineau *et al.,* 1983; Schwarzer and Adams, 1973; Lundien, 1967; Moxham *et al.,* 1965). In this map, the western to northwestern sector is dominated by deep to light blue colours, which suggests weak potassium enrichment and therefore limited hydrothermal influence, consistent with relatively fresh or less altered rocks, which are the sedimentary rocks or sediments (Figure 1). Moving into the central belt, yellow colours become common and form transition patterns between the blue background and the strongest anomalies, which fits alteration halos developed around fluid pathways and structural corridors. The most significant features are the red to pink zones concentrated mainly in the central to eastern part of the map, where high K/Th values indicate strong potassium enrichment relative to thorium and therefore intense hydrothermal alteration. These high zones coincide with the dashed outlines marked as hydrothermal alteration zones, occurring around Bukwium and Tashar Taya, extending toward Anka and the Kagara block, and appearing near Dogon Daji, Tuduki, Gidan Garba, and the Dan Gulbi area. The clustering and locally elongated nature of the red to pink anomalies suggests structurally controlled fluid flow along shear zones and fractures typical of the NW Nigeria schist belts. In terms of mineral exploration, the red to pink cores represent priority targets for gold because gold mineralisation in the region often occurs in shear-hosted quartz veins and altered wall rocks, while the surrounding yellow zones represent the outer alteration envelope that helps define the extent of the system and guides step-out targeting.

Potassium deviation (Kd) map

Figure 6 represents the Kd map of the study area. This map has revealed portions where K is enriched or depleted. Low Kd values that range between blue and green are portions with poor K concentrations. These zones could be rock not affected by alteration activities, surfaces that have undergone weathering, or where K has leached out. The moderate Kd values of colour yellow to orange represent transitional zones and mixed lithologies. High Kd values (red to pink) mark potassium-enriched zones (Eleraki *et al.* 2017; Akinlalu, 2023). These areas suggest strong hydrothermal fluid interaction and alteration halos.

The mapped alteration outlines (dashed polygons) of clusters of red to pink colour showed a coherent belt. The strongest Kd anomalies occur much in the centre of the map to the eastern portion of it, with additional patches in the south and southwest. The NE anomaly geometry suggests structurally controlled alteration, consistent with mineralising fluids moving along regional lineaments. Gold occurrence in the basement terrains often concentrates where hydrothermal fluids react with host rocks near structures forming alteration halos. On this Kd map (Figure 6), the red to pink zones inside the alteration polygons represent priority gold targets because they indicate potassium addition linked to hydrothermal systems and broad alteration halos that often surround vein zones and shear-hosted mineralisation.

The highest-priority target areas are the central belt around Bukwium, Tashar Taya, and Gwashi. The high-priority target areas also include the eastern belt around Anka, Kagara, Dogon Daji, and Tuduki, as well as the southern belt toward Dan Gulbi and Gidan Garba.

F-Parameter Map

Figure 7 represents the F-parameter map of the study area. This map shows where potassium enrichment departs from the normal K, Th, and U background, so it is a direct guide to

hydrothermal alteration intensity. On this map (Figure 7), blue areas represent low F values**,** meaning weak potassium deviation and limited hydrothermal overprint. These low zones dominate much of the northwest and west, around Tambawal, Tabkin Kada, and parts of Tokwatcho, and they reflect relatively fresh or weakly altered rocks where potassium enrichment is not pronounced. Yellow areas represent moderate F values, marking transitional zones with moderate potassium deviation. These belts occur widely across the western to central parts of the area and often reflect mixed lithology or mild alteration overprint. They are important because they commonly form halos around stronger alteration cores, and they help trace pathways of fluid movement away from the main structures. The red to pink areas represent high F values, indicating strong potassium deviation and intense hydrothermal alteration. The most prominent high zones occur in the central corridor around Bukwium, Tashar Taya, Gwashi, and Anka, coinciding with the mapped hydrothermal alteration belt. Additional high zones appear eastward around Kagara, Dogon Daji, and Gidan Garba, as well as in the southern belt near Surimi, matching the circled targets on the map. These red to pink patches are priority targets because strong potassium enrichment commonly reflects potassic and sericitic alteration linked to mineralising fluids, quartz veining, and shear zone activity typical of gold-bearing systems in the NW Nigeria schist belt setting.

Composite hydrothermal alteration map and validation

Figure 8 represents the combined hydrothermal alteration map created using fuzzy logic for the study area. This map has been classified into three classes of hydrothermal alteration intensity, with green as low, yellow as moderate, and red as high. Low zones dominate most of the area and form a widespread background pattern, which suggests large tracts of weakly altered or unaltered rocks mixed with local effects from soil cover and vegetation. Moderate zones occur as halos around the strongest anomalies and as narrow belts, indicating transition areas where alteration affects the host rocks but with lower intensity than

the core zones. High alteration zones, shown in red, occur as clustered patches and elongated streaks. The most prominent concentrations appear in the central sector around Tashar Taya and toward Anka and in the eastern section around Tuduki, Gidan Garba, and Dogon Daji. Additional high zones occur in the south around Surimi and as smaller isolated patches in the southwest near Tungan-Rihi (Figure 8). The angular trend occurrence of the high-alteration (red) bodies suggests structural control, such as shear zones, faults, and fracture corridors that guided fluid flow and focused rock alteration. This is confirmed by overlaying the CET structures on the hydrothermal alteration map of the area (Figure 9). We can see that most of hydrothermally altered zones have one or more structural associations that guided hydrothermal fluid flows leading to the alterations.

The hydrothermal alteration zone map has been validated by overlaying eight (8) active mining sites on the map (Figure 9). Out of the 8 mining sites, six (6) sites, amounting to about 75%, were observed to fall directly on the portion of the high hydrothermal alteration zone map, while the remaining 25% falls on CET structures. This led to the creation of the mineral potential map of the study area (Figure 10), showing moderate potential zones in yellow and the high mineral potential zones in red.

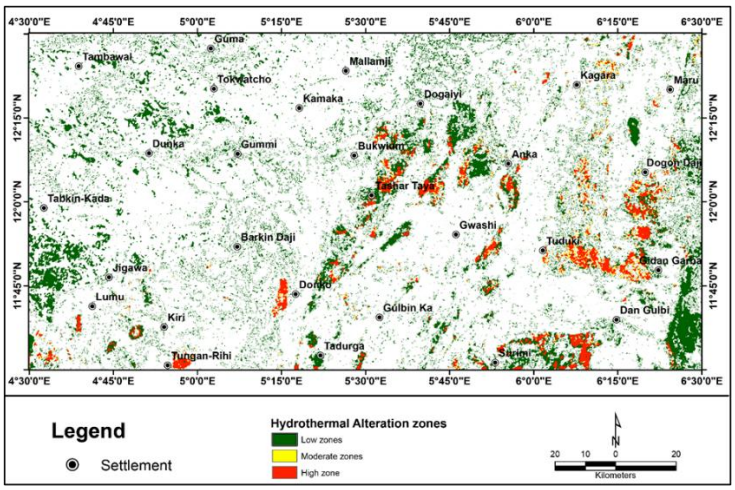

Figure 8: Fuzzy logic combined hydrothermal alteration zones of the study area

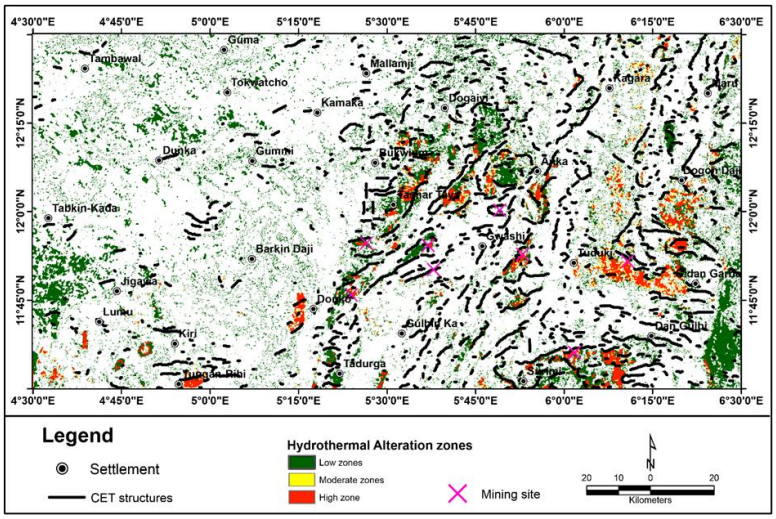

Figure 9: Fuzzy logic combined hydrothermal alteration zones of the study area with CET structures and active mining sites.

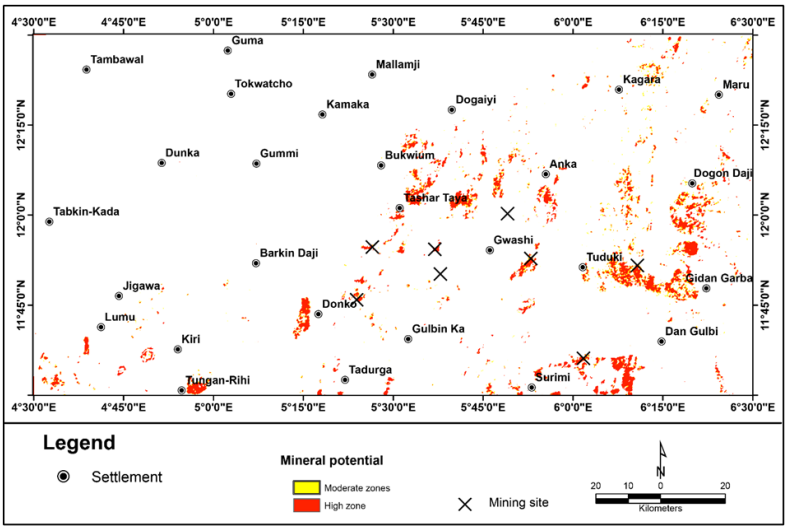

Figure 10: Mineral potential map of the study area

Ternary map and surface geology delineation

To delineate the surface geologic map of the study area, we employed two complementary maps (Figures 11 and 12); the RGB ternary map (Figure 11) is complemented by the CMY ternary map (Figure 12), which were used for surface geological delineation and are effective for anomaly discrimination (Tawey *et al*., 2021; Zhang *et al*., 2017; Duval, 1983).

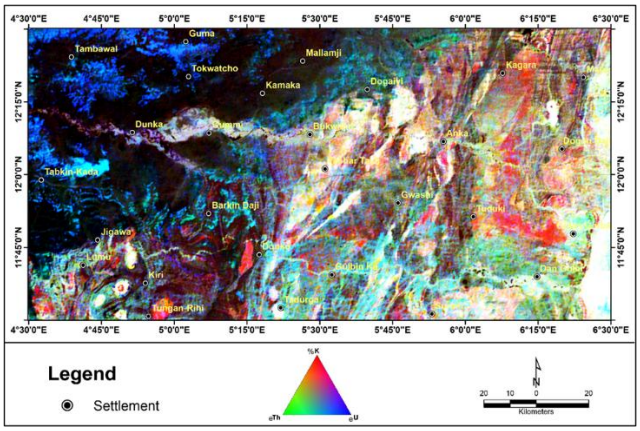

Figure 11: Ternary (RGB) map of the study area

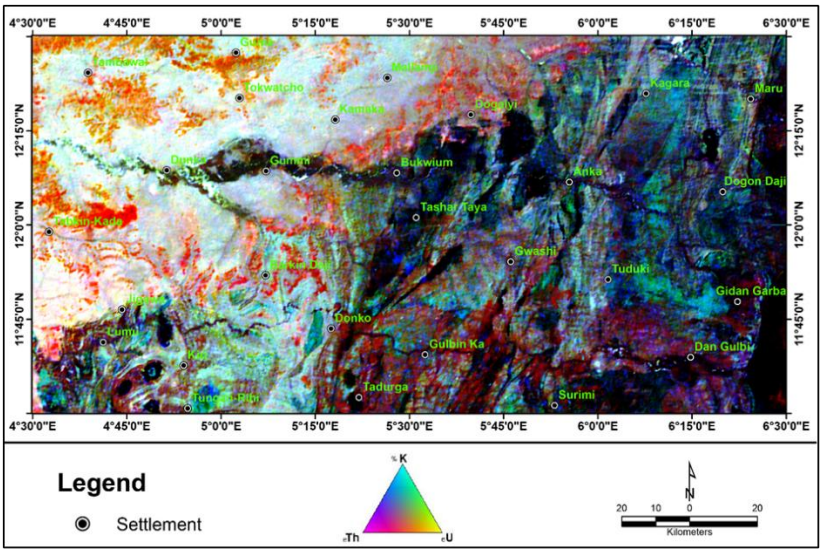

Figure 12: Ternary (CMY) map of the study area

The blue colour portions on the RGB ternary map represent portions with high uranium counts with respect to the other radioelements; so also is the red colour to high potassium counts and green to high thorium counts. Colours beyond these three primary colours represent zones with different proportions of K, Th, and U. Various colours on the ternary map closely correspond to different rock types when compared to the geological map (Figure 1). Based on the geologic map (Figure 1) and ternary map in RGB (Figure 10), we can infer the following: White (high K, Th and U) zones are linked to exposed granitic bedrock and sediments originating from granite. The areas marked in white indicate favourable sites for the exploration of radioelements (Tawey *et al.,* 2021; Akinlalu, 2023). Black to brown zones, characterised by low concentrations of potassium (K), thorium (Th), and uranium (U), are linked to older granites and sediments. Red zones have high K concentrations. Green zones reflect high Th concentrations. Blue zones showed high U concentrations. Cyan zones exhibit high levels of thorium and uranium with low potassium. Magenta areas are marked by high potassium and uranium with low thorium. Yellow regions display high potassium and thorium with low uranium. Certain white zones, noted for high K, Th, and U concentrations and associated with exposed granitic bedrock and granite-derived sediments, are distinctly represented on the CMY map, now appearing dark (black) and readily mappable (Figure 12).

Furthermore, the main lithological units that represent different radioactivity levels have been delineated using the radioelement ternary maps (Figures 11 and 12), and the surface geologic map of the study area was created using the identified lithological units (Figure 13).

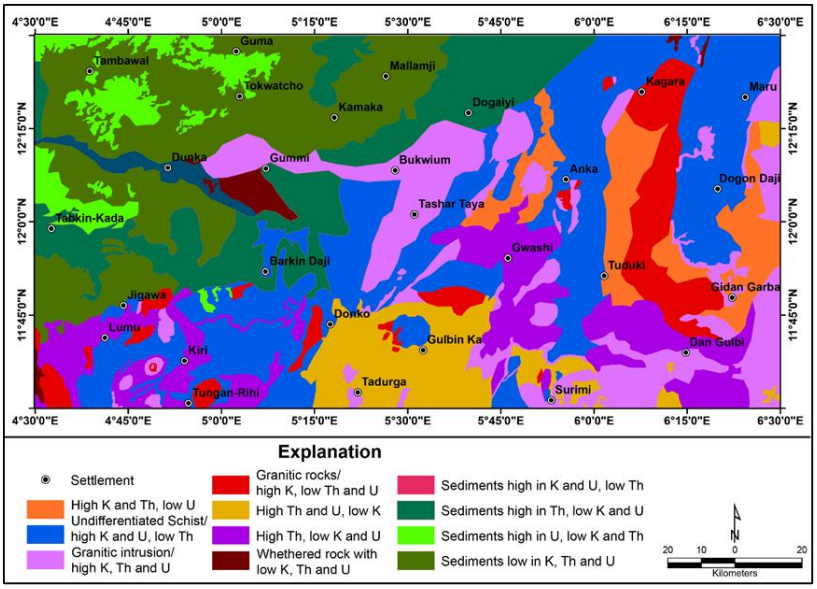

Figure 13: Surface geologic map of the area

V. Discussion

Radiometric responses across the area reflect contrasts between basement rocks and sedimentary cover, plus local hydrothermal overprint. The %K map ranges from low potassium in the western to northwestern sector around Tambawal, Tabkin-Kada, and Jigawa to higher potassium in the east and southeast around Anka, Kagara, Maru, Dogon Daji, Tuduki, and Gidan Garba. A central corridor also shows elevated potassium, trending toward Bukwium and Tashar Taya. Such potassium enrichment fits two controls described in the document: felsic basement lithologies with higher primary K content and potassic alteration linked to mineralising fluids. The eTh map shows higher thorium in several eastern and southeastern belts, with elongated NE to SW trends. Thorium commonly behaves as a relatively immobile element in many alteration settings, so paired interpretation with %K helps separate lithologic background from alteration signatures. The eU map shows lower uranium across much of the western block and increased uranium to the centre and east, with clustered highs around Gummi, Bukwium, Tashar Taya, Anka, Tuduki, Surimi, Dan Gulbi, and Maru flank. Uranium highs support a link to felsic bodies, pegmatites, and fluid-focused enrichment along fracture corridors described for the schist belt terrain.

Hydrothermal alteration mapping relies on three derived indices. The K to Th ratio map shows where potassium has increased compared to thorium. Most of the west and northwest is blue, which points to weak alteration and places where sedimentary cover dominates. Yellow zones mark the change from background to altered ground and often form halos around stronger zones. The red to pink patches stand out as the best targets for potassium enrichment and possible hydrothermal alteration. The strongest K to Th highs group around Bukwium and Tashar Taya stretches toward Anka and shows up again around Kagara, Dogon Daji, Tuduki, Gidan Garba, and Dan Gulbi. On the map, these highs form lines and clusters rather than random spots. This layout suggests fluids moved along shear zones, faults, and fracture networks, which commonly control alteration and mineralisation in Nigerian schist belts. The potassium deviation (Kd) map reinforces these targets by isolating potassium addition relative to local background. Red to pink Kd anomalies define coherent belts in the central and eastern blocks, plus patches toward the south and southwest. Such anomalies fit zones where hydrothermal fluids introduced K feldspar and sericite, producing potassic and sericitic alteration halos around quartz vein systems typical of orogenic gold settings. The F parameter map further tests potassium enrichment relative to combined K, Th, and U behaviour. Low F parameter values cover the northwest and west; moderate values form broad belts across the centre, and high values concentrate in the same central to eastern corridor flagged by K/Th and Kd.

Integration through fuzzy logic weighted overlays produces the composite hydrothermal alteration map with low, moderate, and high classes. High-class zones occur as clustered patches and elongated corridors around Tashar Taya toward Anka, plus eastern clusters near Tuduki, Gidan Garba, and Dogon Daji, with southern highs near Surimi and smaller patches toward the southwest. Validation using active mining sites strengthens the interpretation. Six of the eight sites fall into the high alteration class, with the remaining sites aligning with structures. Radiometric ternary composites support surface geology delineation. RGB ternary mapping separates relative K, Th, and U dominance, while CMY complements anomaly discrimination and improves mapping in high K, Th, and U zones. Comparison with the existing NGSA geological map supports digitising lithologic boundaries and mapping radiometric fingerprints across units, including granitic exposures, granite-derived sediments, and low radioactivity domains associated with older granites and sediments. The combined outputs improve exploration targeting and geological interpretation within the study area.

VI. Conclusion

The aeroradiometric workflow delineated hydrothermal alteration zones and surface geology across parts of the northwest Nigeria schist belts. Radioelement maps show low K, Th, and U responses across much of the western to northwestern sector, with stronger radiometric signatures toward the central and eastern basement-dominated sector. The three alteration indicators, K/Th ratio, potassium deviation, and F parameter, converge on a central to eastern alteration corridor around Bukwium, Tashar Taya, Gwashi, Anka, Kagara, Dogon Daji, Tuduki, Gidan Garba, Dan Gulbi, Surimi, and nearby belts. Many anomalies show elongated geometry consistent with structurally focused hydrothermal fluid pathways. Fuzzy logic integration produces a coherent composite alteration map, and validation against active mining sites shows 75% of sites located within high alteration zones, with the remaining sites linked to mapped structures. Ternary radiometric composites support lithologic discrimination and enable digitising an improved surface geologic map of the study area.

References

[1]. Abaa, S. I. (1983). The Structure And Petrography Of Alkaline Rocks Of The Mada Younger Granite Complex, Nigeria. Journal Of African Earth Sciences, 3, 107-113.

[2]. Ajibade, A. C., Fitches, W. R., And Wright, J. B. (1979). The Zungeru Mylonites, Nigeria: Recognition Of A Major Unit. Revue De Geologie Et De Geographie Physique, 21, 359–363.

[3]. Akame, J. M., Oliveira, E. P., Poujol, M., Hublet, G., And Debaille, V. (2020). LA-ICP-MS Zircon Upb Dating, Luhf, Smnd Geochronology And Tectonic Setting Of The Mesoarchean Mafic And Felsic Magmatic Rocks In The Sangmelima Granite-Greenstone Terrane, Ntem Complex (South Cameroon). Lithos, 372, 105702. Https://Doi.Org/10.1016/J.LITHOS.2020.105702

[4]. Akinlalu, A. A. (2023). Radiometric Mapping For The Identification Of Hydrothermally Altered Zones Related To Gold Mineralization In Ife–Ilesa Schist Belt, Southwestern Nigeria. Indonesian Journal Of Earth Sciences, 3(1), 54-65. Https://Www.Journal.Moripublishing.Com/Index.Php/Injoes/Article/View/519

[5]. Airo, M.-L. (2002). Aeromagnetic And Aeroradiometric Response To Hydrothermal Alteration. Surveys In Geophysics, 23(4), 273–302. Https://Doi.Org/10.1023/A:1015556614694

[6]. Aliyu, A., Ahmed, A. L., And Dewu, M. B. B. (2025). Integrated Airborne Magnetic And Radiometric Data Analysis For The Delineation Of Gold Mineralization Zones In North Central Nigeria. Journal Of Pure And Applied Sciences, 9(1), 33-45. Https://Atbuscienceforum.Com.Ng/Index.Php/Jpas/Article/Download/157/162

[7]. Azzazy, A. A. (2023). Mapping Of Hydrothermal Alteration Zones Around Wadi Zubeir, Northern Eastern Desert, Egypt Using Airborne Gamma-Ray Spectrometric, Aeromagnetic And Remote Sensing Data. 21(1), 21–37. Https://Doi.Org/10.21608/Jegs.2023.385857

[8]. Banfield, J. F. (1985). The Mineralogy And Chemistry Of Granite Weathering. Https://Doi.Org/10.25911/5D666B4212DA7

[9]. Bello, Y., Evans, S. C., Lawal, H., And Alao, J. O. (2025). Investigating Hydrothermal Alteration Associated With Gold Mineralization In Birnin-Gwari Through Transformation Of Aero-Radiometric Data. Proceedings Of The Nigerian Society Of Physical Sciences Conference, 4(1), 45-56. Https://Rans.Nsps.Org.Ng/Index.Php/Pnspsc/Article/View/171

[10]. Boadi, B., Raju, P. S., And Wemegah, D. D. (2022). Analysing Multi-Index Overlay And Fuzzy Logic Models For Lode-Gold Prospectivity Mapping In The Ahafo Gold District–Southwestern Ghana. Ore Geology Reviews, 48, 105059. Https://Doi.Org/10.1016/J.Oregeorev.2022.105059

[11]. Cathelineau, M. (1983). Potassic Alteration In French Hydrothermal Uranium Deposits. Mineralium Deposita, 18(1), 89-97. Https://Doi.Org/10.1007/BF00206697

[12]. Chen, X. (2009). Dynamic Release Of Potassium From Potassium Bearing Minerals As Affected By Ion Species In Solution. Https://En.Cnki.Com.Cn/Article_En/CJFDTOTAL-TURA200906002.Htm

[13]. Chen, Y., Wang, Y., Wang, J., Li, D., Geng, J., Luo, J., And Wang, R. (2025). The Fluid Evolution And Metallogenic Processes Of The Liba Gold Deposit, West Qinling, China: Insights From The Texture, Trace Elements, And H-O Isotope Geochemistry Of Quartz. Minerals, 15(9), 956. Https://Doi.Org/10.3390/Min15090956

[14]. Chiozzi, P., Pasquale, V., Verdoya, M., And Furfaro, V. (2008). Hydrothermal Alteration Inferred From A Radiometric Survey On Lipari (Aeolian Islands, Italy). Environmental Semeiotics, 1(1), 70-82. Https://Doi.Org/10.3383/ES.1.1.5

[15]. Cunha LO, Dutra AC, And Costa AB (2017) Use Of Radiogenic Heat For Demarcation Of Hydrothermal Alteration Zones In The Pernambuco- Brazil. J Appl Geophys 145:111–123

[16]. Doorn, C. J., And Carter, N. Y. (2025). Airborne Geophysics In Wyoming: Methods For Exploring Subsurface Geology.University Of Wyoming. Https://Wyoscholar.Uwyo.Edu/Items/95d45c6b-Fc21-49d9-8bb4-Fcfc28ad102d

[17]. Efimov, A. V. (1978). Multiplikativnyj Pokazatel Dlja Vydelenija Endogennych Rud Poaerogamma-Spektrometriceskim Dannym. Metody Rudnoj Geofiziki. Leningrad, Naucno-Proizvodstvennoje Objedinenie Geofizika.

[18]. Egwuonwu G.N, Ejike, K. N., And Onyekwelu, C. C. (2023). Interpretation Of Radiometric Anomalies Over Some Parts Of The Lower Benue Trough Nigeria, Using High Resolution Aero-Radiometric Data (HRAR). 3(1), 41–50. Https://Doi.Org/10.52589/Ajste-Vnl0q6sa

[19]. El Cheikh, Y., Achkouch, L., Attou, A., Ouchchen, M., Mamouch, Y., Dadi, B., And Rachid, A. (2025). Integrating Heliborne Gamma-Ray Spectrometry And ASTER Satellite Imagery For Enhanced Hydrothermal Alteration And Mineral Prospectivity Mapping: Insights From The Tagragra Of Akka, Morocco. Journal Of Applied Geophysics, 244, 105993. Https://Doi.Org/10.1016/J.Jappgeo.2025.105993

[20]. El-Desoky, H. M., Tende, A. W., Abdel-Rahman, A. M., Ene, A., Awad, H. A., Fahmy, W., El-Awny, H., And Zakaly, H. M. H. (2022). Hydrothermal Alteration Mapping Using Landsat 8 And ASTER Data And Geochemical Characteristics Of Precambrian Rocks In The Egyptian Shield: A Case Study From Abu Ghalaga, Southeastern Desert, Egypt. Remote Sensing, 14(14), 3456. Https://Doi.Org/10.3390/Rs14143456

[21]. Eleraki, M., Ghieth, B., Abd-El Rahman, N., And Zamzam, S. (2017). Hydrothermal Zones Detection Using Airborne Magnetic And Gamma Ray Spectrometric Data Of Mafic/Ultramafic Rocks At Gabal El-Rubshi Area, Central Eastern Desert (CED), Egypt. Advances In Natural And Applied Sciences, 11(9), 182-196.

[22]. Elkhateeb, S. O., And Abdellatif, M. A. G. (2018). Delineation Potential Gold Mineralization Zones In A Part Of Central Eastern Desert, Egypt Using Airborne Magnetic And Radiometric Data. NRIAG Journal Of Astronomy And Geophysics, 7(2), 361-376. Https://Doi.Org/10.1016/J.Nrjag.2018.05.010

[23]. El-Sadek, M. A. (2022). Using Airborne Gamma-Ray Spectrometric Data To The Exposure Of Potassic Alteration -Recognition Of Alteration Relates To Gold Mineralization. Applied Radiation And Isotopes, 190, 110511. Https://Doi.Org/10.1016/J.Apradiso.2022.110511

[24]. El-Qassas, R. A. Y., Abu-Donia, A. M., And Omar, A. E. A. (2023). Delineation Of Hydrothermal Alteration Zones Associated With Mineral Deposits Using Remote Sensing And Airborne Geophysics Data: A Case Study Of El-Bakriya Area, Central Eastern Desert, Egypt. Acta Geodaetica Et Geophysica, 58(2), 339–357. Https://Doi.Org/10.1007/S40328-023-00405-Y

[25]. Gao, S., Xu, H., Li, S.-R., Santosh, M., Santosh, M., Zhang, D., Yang, L., And Quan, S. (2017). Hydrothermal Alteration And Ore-Forming Fluids Associated With Gold-Tellurium Mineralization In The Dongping Gold Deposit, China. Ore Geology Reviews, 80, 166–184. Https://Doi.Org/10.1016/J.OREGEOREV.2016.06.023

[26]. Gobashy, M. M., El-Sadek, M. A., Mekkawi, M. M., Araffa, S. A. S., Ezz Eldin, M. M., And Khalil, M. H. (2024). Radiometric Characteristics Of Some Metallic Ores And Nonmetallic Deposits: An Example, Wadi Al-Allaqi, South Eastern Desert, Egypt. Scientific Reports, 14, Article 2443. Https://Doi.Org/10.1038/S41598-024-52912-9

[27]. Grant, N. K. (1978). Structural Distinction Between Metasedimentary Cover And Underlying Basement In 600 M.Y. Old Pan-African Domains. Geology Society Of American Bulletin. 89, 50-58.

[28]. Green, L. A. (2023). Investigating Geochemical Fluid-Rock Interactions. Scilight. Https://Doi.Org/10.1063/10.0021192

[29]. Lundien JR. (1967) Terrain Analysis By Electromagnetic Means: Laboratory Investigations In The 0- To 2.82 –Mev Gamma-Ray Spectral Region. U.S. Army Engineers Waterways Experiment Station, Vicksburg, Mississippi, Technical Report 3–693;41.

[30]. Macdonald, R., Macdonald, R., Bagiński, B., Kartashov, P. M., And Zozulya, D. (2017). Behaviour Of Thsio4 During Hydrothermal Alteration Of Raremetal Rich Lithologies From Peralkaline Rocks. Mineralogical Magazine, 81(4), 873–893. Https://Doi.Org/10.1180/MINMAG.2016.080.138

[31]. Mamudu, A., Akanbi, E. S., And Odewumi, S. C. (2024). Hydrothermal Alteration And Mineral Potential Zones Of Bauchi Area Northeastern Nigeria Using Interpretation Of Aeroradiometric Datas. Journal Of Nigerian Society Of Physical Sciences, 2193. Https://Doi.Org/10.46481/Jnsps.2025.2193

[32]. Mccurry, P. (1976). The Geology Of The Precambrian To Lower Palaeozoic Rocks Of Northern Nigeria. A Review. In: Kogbe CA (Ed) Geology Of Nigeria. Lagos: Elizabethan Publishers, 15-39

[33]. Meng, Y. (2013). Research On Geochemical Characteristics Of Thorium For Julong,An Deposit,Xiangshan Ore Field. Geological Journal Of China Universities. Https://En.Cnki.Com.Cn/Article_En/CJFDTOTAL-GXDX201301018.Htm

[34]. Meng, L. (1999). Silicification And Mineralization In Hydrothermal Deposits. Chinese Science Bulletin, 44(1), 90–93. Https://Doi.Org/10.1007/BF03182895

[35]. Moxham, R. M., Foote, R. S., And Bunker, C. M. (1965). Gamma-Ray Spectrometer Studies Of Hydrothermally Altered Rocks. Economic Geology, 60(4), 653–671. Https://Doi.Org/10.2113/GSECONGEO.60.4.653

[36]. Murphy, T. (2025). Using Gamma-Ray Spectrometry To Map A Granite-Sandstone Contact On Mason Mountain WMA, Texas. Texas Aandm University, Master's Thesis. Https://Oaktrust.Library.Tamu.Edu/Items/34e516e6-7ef0-4d85-Bd27-5f7652317ad4

[37]. Nabighian, M. N., Grauch, V. J. S., Hansen, R. O., Lafehr, T. R., Li, Y., Peirce, J. W., Phillips, J. D., And Ruder, M. E. (2005). The Historical Development Of The Magnetic Method In Exploration. Geophysics, 70(6), 33ND–61ND. Https://Doi.Org/10.1190/1.2133784

[38]. Nisbet, H., Nisbet, H., Migdisov, A., Williams-Jones, A. E., Xu, H., Van Hinsberg, V. J., And Roback, R. (2019). Challenging The Thorium-Immobility Paradigm. Scientific Reports, 9(1), 17035. Https://Doi.Org/10.1038/S41598-019-53571-X

[39]. NGSA. Geology And Structural Lineament Map Of Nigeria; 2006

[40]. Obaje NG. Geology And Mineral Resources Of Nigeria, Berlin: Springer-Verlag, Heidelberg. 2009;221

[41]. Ohwo, M. U., And Solape, F. S. (2024). Integration Of ASTER And Airborne Radiometric Data In The Exploration For Hydrothermal Alteration Zones Associated With Mineral Deposits In Igarra Schist Belt. International Journal Of Earth Sciences Knowledge And Applications, 6(1), 23–38. Https://Dergipark.Org.Tr/En/Pub/Ijeska/Issue/87240/1553919

[42]. Ondrejka, M., Förster, H., Bévan, M., Uher, P., Kianguebene-Koussingounina, C. E., And Mahdy, N. M. (2025). Evolution Of Accessory Nb–Ta–W–Sn–Ti–Fe Oxide Minerals From The Markersbach Highly Evolved Aluminous A-Type Granite, Erzgebirge, Germany: Magmatic To Hydrothermal Processes And Elemental Mobility During F-Rich Fluid–Rock Interaction. Geologica Carpathica, 76(3). Https://Doi.Org/10.31577/Geolcarp.2025.14

[43]. Oyarzabal, J. C., Galliski, M. A., And Perino, E. (2009). Geochemistry Of K-Feldspar And Muscovite In Rare-Element Pegmatites And Granites From The Totoral Pegmatite Field, San Luis, Argentina. Resource Geology, 59(4), 315–329. Https://Doi.Org/10.1111/J.1751-3928.2009.00100.X

[44]. Pe-Piper, G., Jansa, L. F., And Palacz, Z. (1994). Geochemistry And Regional Significance Of The Early Cretaceous Bimodal Basalt-Felsic Associations On Grand Banks, Eastern Canada. Geological Society Of America Bulletin, 106(10), 1319–1331. Https://Doi.Org/10.1130/0016-7606(1994)106<1319:GARSOT>2.3.CO;2

[45]. Pliler, R., And Adams, J. A. S. (1962). The Distribution Of Thorium, Uranium, And Potassium In The Mancos Shale. Geochimica Et Cosmochimica Acta, 26(11), 1115–1135. Https://Doi.Org/10.1016/0016-7037(62)90048-0

[46]. Reford, S. W., Misener, D. J., Ugalde, H. A., Gana, J. S., And Olaniyan, O. (2010). Nigeria's Nationwide High-Resolution Airborne Geophysical Surveys, Conference. Society Of Exploration Geophysicists (SEG) Technical Program Expanded Abstracts.1835-1839. Https://Doi.Org/10.1190/1.3513199.

[47]. Qiu, K.-F., Romer, R. L., Yu-Long, Z., Yu, H.-C., Turner, S., Wan, R.-Q., Li, X., Gao, Z.-Y., And Deng, J. (2024). Potassium Isotopes As A Tracer Of Hydrothermal Alteration In Ore Systems. Geochimica Et Cosmochimica Acta. Https://Doi.Org/10.1016/J.Gca.2024.01.005

[48]. Rao, M. (2012). The Geochemical Characteristics Of Alkali Metasomatic Ore And Its Ore-Forming Significance At Zoujiashan Deposit, Xiangshan Uranium Field. Uranium Geology.

[49]. Ratajeski, K., Glazner, A. F., And Miller, B. V. (2001). Geology And Geochemistry Of Mafic To Felsic Plutonic Rocks In The Cretaceous Intrusive Suite Of Yosemite Valley, California. Geological Society Of America Bulletin, 113(11), 1486–1502. Https://Doi.Org/10.1130/0016-7606(2001)113<1486:GAGOMT>2.0.CO;2

[50]. Sabins, F. F. (1999). Remote Sensing For Mineral Exploration. Ore Geology Reviews, 14(3-4), 157-183. Https://Doi.Org/10.1016/S0169-1368(99)00007-4

[51]. Saikia, A., Gogoi, B., Ahmad, M., And Ahmad, T. (2014). Geochemical Constraints On The Evolution Of Mafic And Felsic Rocks In The Bathani Volcanic And Volcano-Sedimentary Sequence Of Chotanagpur Granite Gneiss Complex. Journal Of Earth System Science, 123(5), 959-987. Https://Doi.Org/10.1007/S12040-014-0455-7

[52]. Santiago Ramos, D. P., Nielsen, S. G., Coogan, L. A., Scheuermann, P. P., Seyfried, W. E., And Higgins, J. A. (2022). The Effect Of High-Temperature Alteration Of Oceanic Crust On The Potassium Isotopic Composition Of Seawater. Geochimica Et Cosmochimica Acta, 339, 1–11. Https://Doi.Org/10.1016/J.Gca.2022.10.013

[53]. Sanusi, S. O., And Amigun, J. O. (2020). Structural And Hydrothermal Alteration Mapping Related To Orogenic Gold Mineralization In Part Of Kushaka Schist Belt, North-Central Nigeria, Using Airborne Magnetic And Gamma-Ray Spectrometry Data. SN Applied Sciences, 2, 1-26. Https://Doi.Org/10.1007/S42452-020-03435-1

[54]. Schwarzer TF, And Adams JAS (1973). Rock And Soil Discrimination By Low Altitude Airborne Gamma-Ray Spectrometry In Payne County, Oklahoma. Economic· Geology.68: 1297-1312

[55]. Shives RK, Charbonneau BW And Ford KL (1997) The Detection Of Potassic Alteration By Gamma-Ray Spectrometry-Recognition Of Alteration Related To Mineralization. In A. G. Gubins (Ed.), Proceedings Of Exploration 97: Fourth Decennial International Conference On Mineral Exploration, Pp 741-752

[56]. Stoch, L., And Sikora, W. (1976). Transformations Of Micas In The Process Of Kaolinitization Of Granites And Gneisses. Clays And Clay Minerals, 24(4), 156–162. Https://Doi.Org/10.1346/CCMN.1976.0240402

[57]. Tawey, M. D., Adetona, A. A., Alhassan, U. D., Rafiu, A. A., Salako, K. A., And Udensi, E. E. (2021). Aeroradiometric Data Assessment Of Hydrothermal Alteration Zones In Parts Of North Central Nigeria. Asian Journal Of Geological Research, 4(2), 1-16.

[58]. Truswell, J.F, And Cope, R.N (1963) The Geology Of Parts Of Niger And Zaria Provinces, Northern Nigeria. Geol Suvey Nigeria Bull 29:1–104

[59]. Tulepbayev, K., And Tulemissova, Z. S. (2025). Hydrothermal Alteration And Mineralogical Zonation At The Bozshakol Porphyry Copper Deposit: Integration Of Spectral, Magnetic, And 3d Modeling Data. Ķazaķstan-Britan Tehnikalyķ Universitetìniņ Habaršysy, 22(3), 356–369. Https://Doi.Org/10.55452/1998-6688-2025-22-3-356-369
[60]. Turner DC (1983) Upper Proterozoic Schist Belts In The Nigerian Sector Of The Pan-African Province Of West Africa. Precambrian Res 21:55–79
[61]. Wright, J. B. (1985). Geology And Mineral Resources Of West Africa. George Allen And Unwin, London. 187.
[62]. Yılmaz, K. (2019). Geochemistry Of Ultramafic, Mafic, And Felsic Xenoliths From The Gölcük (Isparta, SW Turkey) Alkali Rocks: Genetic Relationship With Arc Magmas. Arabian Journal Of Geosciences, 12(9), 1–16. Https://Doi.Org/10.1007/S12517-019-4461-6
[63]. Zaccarini, F., Baumgartner, R. J., Mavrogonatos, C., And Garuti, G. (2025). Magmatic Significance And Hydrothermal Alteration Of Layered Chromitites From The Bracco Gabbro Complex Ophiolite, Ligurian Ophiolites, Italy. Bulletin Of The Mineral Research And Exploration, 178(178), 1–2. Https://Doi.Org/10.19111/Bulletinofmre.1764813
[64]. Zhang, X., Beard, B. L., Neuman, M., Fahnestock, M. F., Bryce, J. G., And Johnson, C. M. (2022). Stable Potassium (K) Isotope Characteristics At Mid-Ocean Ridge Hydrothermal Vents And Its Implications For The Global K Cycle. Earth And Planetary Science Letters, 593, 117653. Https://Doi.Org/10.1016/J.Epsl.2022.117653